Journal of Quantitative Spectroscopy & Radiative Transfer 264 (2021) 107546

Contents lists available at ScienceDirect

Journal of Quantitative Spectroscopy & Radiative Transfer

journal homepage: www.elsevier.com/locate/jqsrt

Speed-dependent broadening of the O_2 fine-structure lines

M.A. Koshelev[a,*], I.N. Vilkov[a], D.S. Makarov[a], M.Yu. Tretyakov[a], P.W. Rosenkranz[b]

[a] IAP RAS, 46 Ulyanov Str., 603950 Nizhny Novgorod, Russia
[b] Massachusetts Institute of Technology, Cambridge, MA 02139, USA

ARTICLE INFO

Article history:
Received 26 November 2020
Revised 28 January 2021
Accepted 28 January 2021
Available online 1 February 2021

Keywords:
Speed dependent effects
Molecular oxygen
Atmospheric microwave absorption model
Line shape
Collisional broadening

ABSTRACT

Pressure broadening of the molecular oxygen fine-structure lines near 60 GHz was experimentally reexamined in the range of rotational quantum numbers up to N=39, in the pure gas at room temperature. The analysis of a representative set of individual line profiles with N varying from 1 to 21 included the speed dependence of collisional relaxation, which affects absorption by 0.25–0.5% of maximum at low pressures. The ratio of the two speed-dependence parameters γ_0 and γ_2 exhibits no notable variation with N. Obtained data are compared with similar parameters of other oxygen bands in the near-infrared and visible spectral ranges. Assuming similar speed dependence in air as for pure oxygen, we find that at 1-atm pressure, the impact of introducing speed-dependent line mixing and broadening coefficients into a model for the atmospheric oxygen 60-GHz band is 0.05–0.1% of maximum absorption, much smaller than the influence of either first- or second-order speed-independent line mixing.

1. Introduction

Information on the millimeter wave spectrum of the O_2 molecule is important for applications related to remote sensing of the atmosphere. The most common ground-based microwave radiometer profilers operate in the 20–60 GHz range to infer climate variables such as tropospheric temperature and water vapor profiles [1]. The main constituents contributing to the atmospheric microwave radiation absorption in the 20-60 GHz range are water vapor and oxygen. Generally, absorption of oxygen is provided by a large number of fine-structure magnetic-dipole transitions. Absorption models usually take into account a few dozen of these lines (*e.g.* [2]). The fine-structure lines are mostly located within ±10 GHz around 60 GHz, with one line lying apart at 118.75 GHz. At low pressures the lines are well resolved. With increasing pressure, the lines broaden and merge, forming the absorption band. The band profile cannot be modelled as a sum of isolated line profiles due to their distortion by the line-mixing effect [2–8].

In our earlier studies [9–12] precise values of the line central frequencies, broadening coefficients and their dependencies on temperature and rotational quantum state were measured using different experimental techniques. The mixing of the oxygen fine-structure lines was also studied by us at high pressure for both the single 118-GHz line [10,13–15], and the 60-GHz band [9,16,17]. Our results were used for updating the Millimeter wave propagation model (MPM) [18]. The typical magnitude of the mixing-effect contribution at room temperature and atmospheric pressure is about 20% for the 60-GHz band and about 0.5% for the line at 118.75 GHz.

To the best of our knowledge, there are no models of atmospheric absorption of millimeter-wave radiation that take into account the influence of the “wind effect” (speed dependence (SD) of the collisional relaxation rate of the absorbing molecules) on the 60-GHz oxygen band. The SD effect manifests itself in a minor deviation of the line profile from the classical Voigt model, which is not easy to observe for weak magnetic-dipole transitions of O_2. The only data available in the microwave is from our recent experimental study [15] where manifestation of the SD effect was demonstrated and investigated for the 118.75 GHz line. No lines of the 60-GHz band were studied in this way. However, neglecting the SD effect might lead to systematic errors in retrieval of atmospheric parameters from remote sensing data [19].

The purpose of the current study is the quantitative characterisation of the “wind effect” impact on the individual profiles of the 60-GHz band lines at room temperature and low pressures, and further evaluation of the effect on the whole band profile near 1-atm pressure. Section 2 describes the experimental details, Section 3 shows the result of the experimental data analysis and a comparison with the values acquired for other bands, and Section 4 provides an evaluation of the “wind effect” contribution to the profile of the 60-GHz band.

* Corresponding author.
E-mail address: koma@ipfran.ru (M.A. Koshelev).

https://doi.org/10.1016/j.jqsrt.2021.107546
0022-4073/

2. Experiment

Line profiles were recorded by means of a spectrometer with a backward-wave oscillator (BWO) and radio-acoustic detection of the absorption, used in our previous studies (see [15] and [9,12,20,21] for the details). High sensitivity of the radio-acoustic cell in the spectrometer is achieved at its relatively small size (2 cm diameter and 10 cm length). This facilitates improving the cell thermal and mechanical isolation, thus reducing the instrumental noise level and allowing detection of weak absorption. The copper cell was placed into a double magnetic permalloy shield to avoid distortions of the shape of the magnetic-dipole oxygen transitions by external magnetic fields. Frequency manipulation of the BWO radiation at the rate of 80 Hz with a precisely fixed deviation was applied by means of a phase-locking loop. The value of the deviation was set to be approximately equal to the line half-width at half-maximum (HWHM). The difference in the gas absorption at frequencies defined by the BWO frequency manipulation causes variations of pressure in the cell, which are registered by the capacitive microphone. The signal is further acquired by the digital lock-in amplifier with reference frequency equal to the manipulation frequency. The observed line shape can be modelled as

$$S(\nu) = F(\nu + d) - F(\nu - d) \quad (1)$$

where $F(\nu)$ is the regular line shape (Lorenz, Voigt, *etc.*), which is used in the case of amplitude modulation, and d is a deviation.

Profiles of the O_2 fine structure lines were recorded at pressures ranging from 0.1 up to 2.8 Torr and accurately controlled room temperature. Each recording contained 201 frequency points (acquisition time was 0.5 s per point) covering the interval of about 25 half-widths around the line center. Multiple (up to 100) spectra were accumulated and further averaged. The resulting signal-to-noise ratio (SNR) of the experimental spectra reached the value of 5600 for the most intense lines of the band.

We used an oxygen sample from the local supplier, with specified purity not worse than 99.999%. The temperature of the cell was monitored by means of three copper temperature sensors of ±0.5 K stated uncertainty, mounted on the cell surface. Temperature gradients were estimated to be zero within the sensors' uncertainties. Gas pressure in the cell was permanently monitored using a 10-Torr-range pressure gauge (MKS Baratron type 626B) having uncertainty of ~0.2% of the reading. Room air conditioning provided temperature stability of the whole setup within ±0.5 K during each experimental day.

3. Data treatment

Two line shape models were employed for the spectra analysis. A Voigt profile (VP) which is characterized by the collisional width $\Gamma = \gamma \cdot p$ at pressure p was used for all recordings to make a comparison of the results of the current and previous studies possible. For ten lines (see Table 1) spectra recordings having sufficient SNR were analyzed using the HTP model in the quadratic speed-dependent Voigt (qSDVP) limit (see [22,23] for details). Dependence of the collisional width Γ on absorbing molecule speed v is described in the model by the quadratic function [24,25]:

$$\Gamma(v) = \Gamma_0 + \Gamma_2\left[\left(\frac{v}{\tilde{v}}\right)^2 - \frac{3}{2}\right] \quad (2)$$

with the most probable speed $\tilde{v} = \sqrt{2k_BT/m}$ for the absorbing molecule having mass m at temperature T; k_B is Boltzmann's constant. Here $\Gamma_0 = \gamma_0 \cdot p$ is the collisional half-width averaged over all relative speeds ку, at pressure p, and $\Gamma_2 = \gamma_2 \cdot p$ determines the speed-dependent part of the collisional half-width.

Table 1
Pressure broadening parameters recalculated to 296 K using experimental temperatures T_{exp} (last column), power law and temperature exponent $n_\gamma = 0.765(11)$ from Koshelev et al. [12].

Line* N	Voigt	speed-dependent Voigt			T_{exp} (K)
	γ MHz/Torr	γ_0 MHz/Torr	γ_2 MHz/Torr	γ_2/γ_0 Unitless	
1−**	2.244(7)	2.274(7)	0.172(12)	0.076(6)	296.5
3−	2.082(6)	2.093(6)	0.138(3)	0.066(2)	298.6
3+	2.018(6)	–	–	–	300.5
5−	1.923(5)	1.940(6)	0.123(3)	0.063(2)	296.4
5+	1.900(5)	1.909(5)	0.098(3)	0.051(2)	297.8
7−	1.838(5)	–	–	–	296.9
7+	1.823(5)	1.840(5)	0.132(3)	0.072(2)	296.3
9−	1.810(5)	1.829(5)	0.147(5)	0.080(3)	296.0
9+	1.793(5)	1.812(5)	0.138(5)	0.076(3)	296.0
11−	1.755(5)	–	–	–	297.9
11+	1.748(5)	1.760(5)	0.109(3)	0.062(2)	299.8
13+	1.703(5)	1.715(4)	0.085(3)	0.050(2)	297.2
15+	1.664(5)	1.677(4)	0.094(3)	0.056(2)	297.0
17+	1.626(5)	–	–	–	296.5
19−	1.590(11)	–	–	–	296.0
21+	1.548(5)	1.558(5)	0.100(5)	0.064(3)	300.2
23−	1.504(10)	–	–	–	296.0
25+	1.446(10)	–	–	–	296.0
27−	1.406(18)	–	–	–	296.7
29+	1.343(10)	–	–	–	296.0
31+	1.306(23)	–	–	–	295.5
33+	1.257(18)	–	–	–	296.0
35+	1.195(12)	–	–	–	296.0
37+	1.144(14)	–	–	–	296.0
39+	1.090(18)	–	–	–	296.0

* Standard line notation is used (see *e.g.* [7]).
** Parameters and errors for the 1− line are from Koshelev et al. [15].

The spectra analysis applied a multifit procedure, in which the model function was fitted simultaneously to all experimental recordings of a chosen line. Expected linear pressure dependencies of Γ_0 and Γ_2 were considered.

The result of the multifit analysis of the line $N = 11+$ is shown in Fig. 1 as a typical example. Fit residuals demonstrate the impossibility of the VP to reproduce the experimental spectra within the noise level. Employing qSDVP leads to significantly better agreement with the recorded spectra. Small distortions in the qSDVP fit residuals at lowest pressures could be caused by the residual magnetic fields. Spectra corresponding to pressures below 0.5 Torr had poorer SNR due to decreased spectrometer sensitivity and were not included in the multifit analysis by qSDVP. Results from both VP- and qSDVP-fits were used for further analysis and comparison to the earlier measurements.

Table 1 shows derived pressure broadening parameters recalculated to 296 K using experimental temperatures (last column), exponential law and temperature exponent $n_\gamma = 0.765(11)$ from the earlier study [12]. Errors given in parentheses correspond to a combined total uncertainty (except for the 1− line) which was calculated as a square-root of the sum of squared errors: 3σ fit uncertainties, pressure- and temperature-related uncertainties. Fig. 2 shows Voigt broadenings γ from Table 1 in comparison with our earlier results [9] and [12].

All the data presented in Fig. 2 for the 60-GHz lines are mainly in good agreement within the combined uncertainties. Some difference is observed between broadening coefficients of $N+$ and $N-$ lines, namely $N-$ lines are systematically wider than $N+$ lines. The maximum difference, about 3%, is observed for the 3− and 3+ lines. Since this tendency is observed in all datasets presented, it might have a physical origin and should be considered in band-shape modelling for better accuracy.

Dependence of the pressure broadening parameters of oxygen fine-structure lines on rotational quantum number N was analyzed

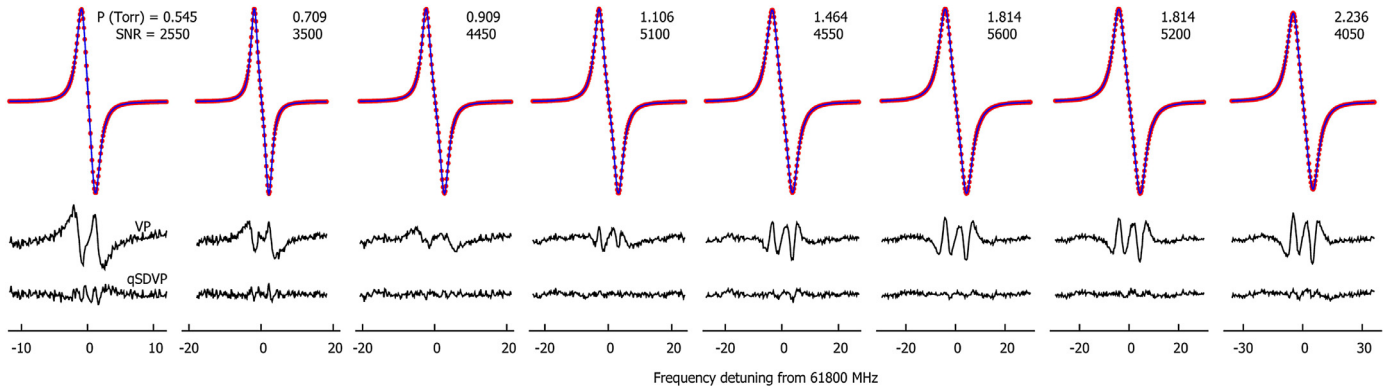

Fig. 1. Recorded profiles of the line $N = 11+$ at 61.8002 GHz at various pressures ($T = 299.8$ K). Residuals of the VP and qSDVP fitted to all recordings simultaneously are shown in the lower part of the figure upscaled by a factor of 100.

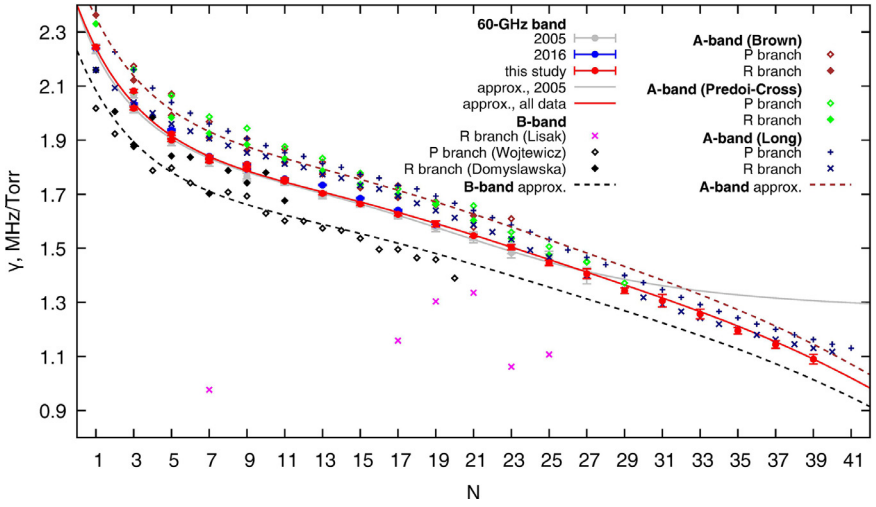

Fig. 2. Self-broadening coefficients γ from current and earlier [9,12] studies compared to those for the B-band [26–28] and A-band [29–31]. Smooth lines are Padé approximants for the 60-GHz data. The approximants for the A-band and B-band line broadenings are obtained by scaling the red curve for the 60-GHz band by a factor of 1.05 and 0.93, respectively.

earlier [12] using the Padé approximation

$$\gamma(N) = A_\gamma + \frac{B_\gamma}{1 + \sum c_i N^i} \tag{3}$$

Experimental data from [9] with maximum $N = 27$ were used. Despite the contribution of the high-N lines being weak, the MPM [18], model of atmospheric absorption, currently accounts for the lines up to $N = 37$. In this study, self-broadening was measured for the lines up to $N = 39$. Typical recordings of weak lines are presented in Fig. 3. It is worth noting that the weakest line studied, 39+, has the intensity $2.67{\cdot}10^{-29}$ cm/molec [32] and was recorded with SNR∼35 (averaging over 120 scans). The corresponding value of the spectrometer sensitivity in terms of absorption coefficient is about $2{\cdot}10^{-10}$ cm^{-1} (or $3{\cdot}10^{-8}$ cm^{-1}Hz$^{-0.5}$) at 10-20 mW radiation power.

The rotational dependence of the self-broadening parameters of oxygen lines was refined (Table 2) using all our data for the 60-GHz lines presented in Fig. 2. Measured pressure broadening parameters are reproduced by the Padé approximation Eq. (3) with a standard deviation of ±0.015 MHz/Torr. We note that extrapolation properties of Eq. (3) with parameters from Table 2 may be poor. Fig. 2 demonstrates that the difference between the earlier and refined dependencies $\gamma(N)$ is mainly observed above $N = 27$, reaching about 20% for $N = 39$.

The self-broadening parameters γ of the corresponding lines of the A-band [29–31] and B-band [26–28] shown in Fig. 2 differ systematically from the microwave data but demonstrate similar rotational dependence. The Padé approximant for the 60-GHz band data, scaled by the factor of 1.05 and 0.93, seems to be suitable for the self-broadening coefficients of the A-band and B-band lines, respectively.

Profiles of the lines 3–, 5+, 5–, 7+, 9–, 9+, 11+, 13+, 15+ and 21+ were analyzed using VP and qSDVP models to derive both the "classical" self-broadening parameter γ and SD-model parameters γ_0 and γ_2 (Table 1). Fig. 4 shows obtained values of γ_0 in comparison to those for the A-band [30,33] and B-band [26–28].

Fig. 5 shows ratios γ/γ_0, complemented by 1− line data from our earlier study [15]; they appear to be independent of N within the experimental uncertainty. Ratios γ/γ_0 for the corresponding lines of the A-band [30] and B-band [26,27,34] are also shown in Fig. 5. The A-band ratios are close to those of the current study, while the B-band data are significantly lower and their use for modelling the 60-GHz band profile would overestimate the SD-effect.

Fig. 6 compares the γ_2/γ_0 ratio for the 60-GHz band and three electronic bands: A-band [33], B-band [26–28] and 1.27 μm band [35] (only dipole transitions are considered). Ratios γ_2/γ_0 for all infrared bands are systematically higher and show rotational dependence, increasing as N increases. The difference between mm-wave and other bands data varies on average from 20% for low-N lines to about 3 times for high-N lines. Therefore, using the parameters of the electronic bands for the 60-GHz band would give significant overestimation of the SD-effect and incorrect band shape.

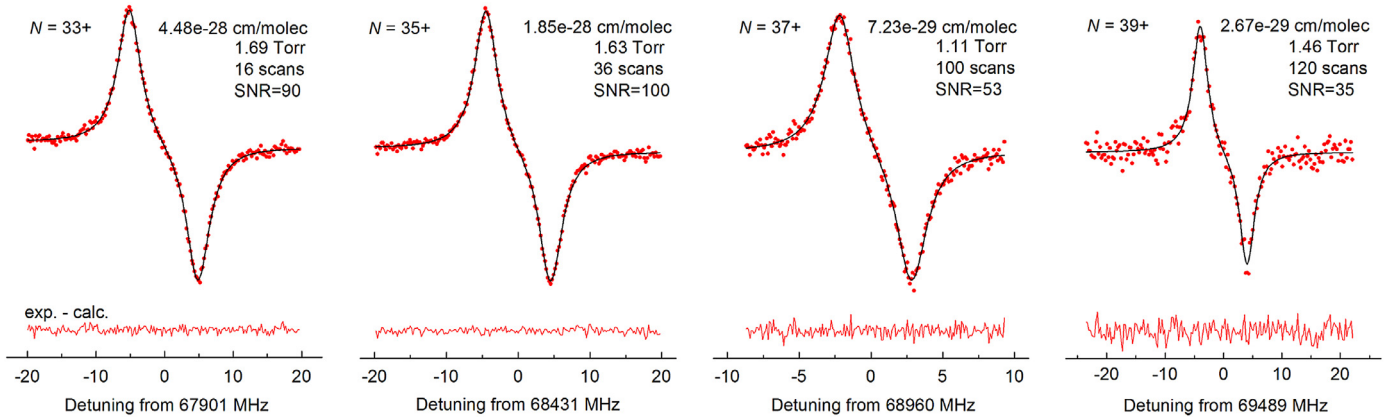

Fig. 3. Recordings of the lines 33+, 35+, 37+ and 39+ and corresponding residuals of the fitted VP model.

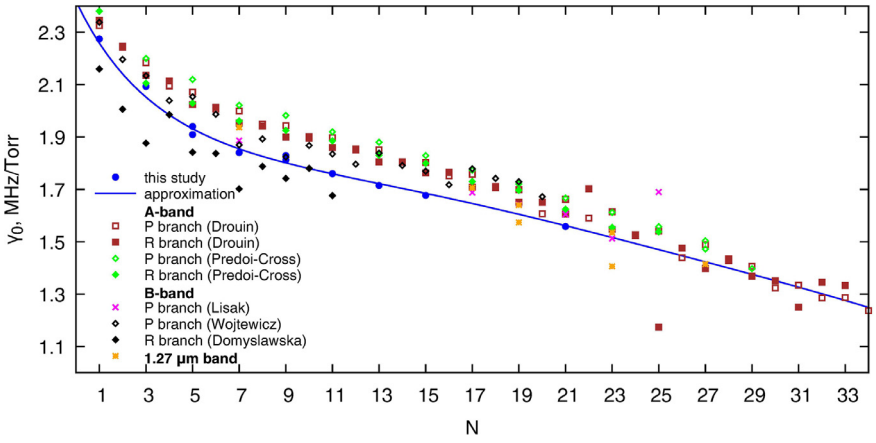

Fig. 4. Self-broadening coefficients γ_0 from the SD-model retrieved in current study (Table 1) compared to ones for the B-band [26–28], A-band [30,33] and 1.27 μm band [35]. Padé approximant for the 60-GHz band lines is obtained by scaling the corresponding dependence for γ, shown by the red curve in Fig. 2, by the factor of 1.008.

Table 2
Results of the weighted fit of Eq. (3) to the measured broadening coefficients $\gamma(296)$.

Parameter	From [12]	This study
A_γ	1.263	0.2499
B_γ	1.129	2.1588
c_1	0.186	0.09298
c_2	-0.0071	-0.00904
c_3	0*	$4.985 \cdot 10^{-4}$
c_4	$1.249 \cdot 10^{-5}$	$-1.225 \cdot 10^{-5}$
c_5	0*	$1.162 \cdot 10^{-7}$

* Fixed to zero.

Thus the comparison with other data allows us to draw the following two conclusions:

(1) Collisional broadening of oxygen lines is band-dependent. This is confirmed by general coincidence of the repeated measurements (including measurements by different authors and different techniques) within the same band and systematic deviation of data from band to band. In our opinion, this deviation is related, first of all, to the basic properties of the intermolecular interaction potential and to the imperfect approximation of the SD effect by the quadratic function (2) demonstrated previously for a number of molecules (see, *e.g.*, Fig. 8 in [36] for OCS, Fig. 4 in [37] for H_2O).

(2) Systematic measurement errors are prominent in data related to the SD parameter γ_2. This is evidenced by the fact that the spread of experimental points relative to the expected smooth dependence of this parameter on a rotational quantum number is in most cases significantly larger than the quoted measurement errors.

The ratio γ_2/γ_0 for the lines of the 60-GHz band does not reveal any noticeable rotational dependence, so the averaged values $\gamma/\gamma_0 = 0.992(2)$ and $\gamma_2/\gamma_0 = 0.062(6)$ will be used to calculate speed-dependent collisional parameters for all fine structure lines of the band included into absorption models (these averaged values are shown by the dashed lines in Figs. 5 and 6). For the 1− line, as it stands apart and is well resolved at any atmospheric conditions, values derived directly from the experiment [15] will be used.

4. SD-effect manifestation in the 60-GHz band at atmospheric pressure

The profile of the 60-GHz oxygen band can be computed by the millimeter wave propagation model (MPM). Fortran code is available from [38]. Oxygen absorption is modeled in the range up to 1 THz using a line-by-line approach, taking into account 44 oxygen lines (38 of which correspond to fine-structure transitions). The latest version [17] uses the Van Vleck–Weisskopf line shape modified with first- and second-order corrections for line mixing [2,5,6] (VVWLM profile). In this model, a self-consistent set of the parameters was obtained by fitting the mixing coefficients to laboratory measurements at 1-atm pressure, considering line intensities and broadening coefficients as fixed parameters. Any change to the broadening coefficients (*e.g.*, replacing γ by γ_0) of the collisionally-coupled oxygen lines requires the mixing coeffi-

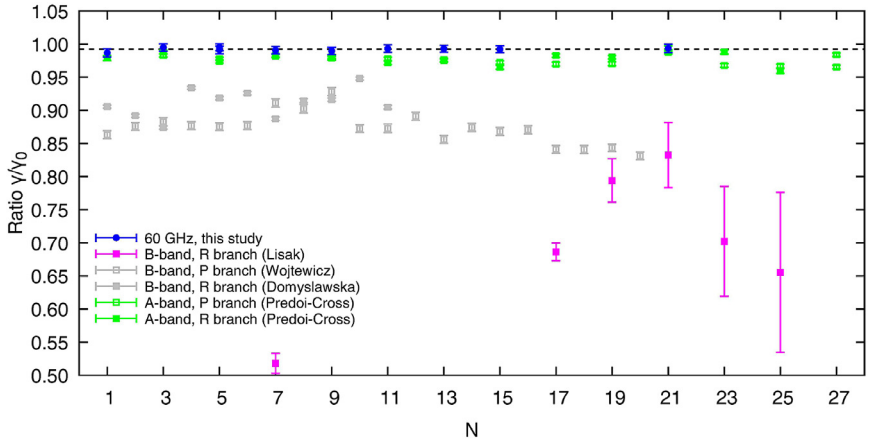

Fig. 5. Ratios γ/γ_0 for various fine-structure oxygen lines (blue circles). Values for $N = 1-$ line are taken from our earlier study [15]. Similar ratios for the lines of the B-band [26,27,34] and A-band [30] are shown by squares (see legend in the figure). Dashed line shows averaged ratio value 0.992(2) for the 60-GHz band.

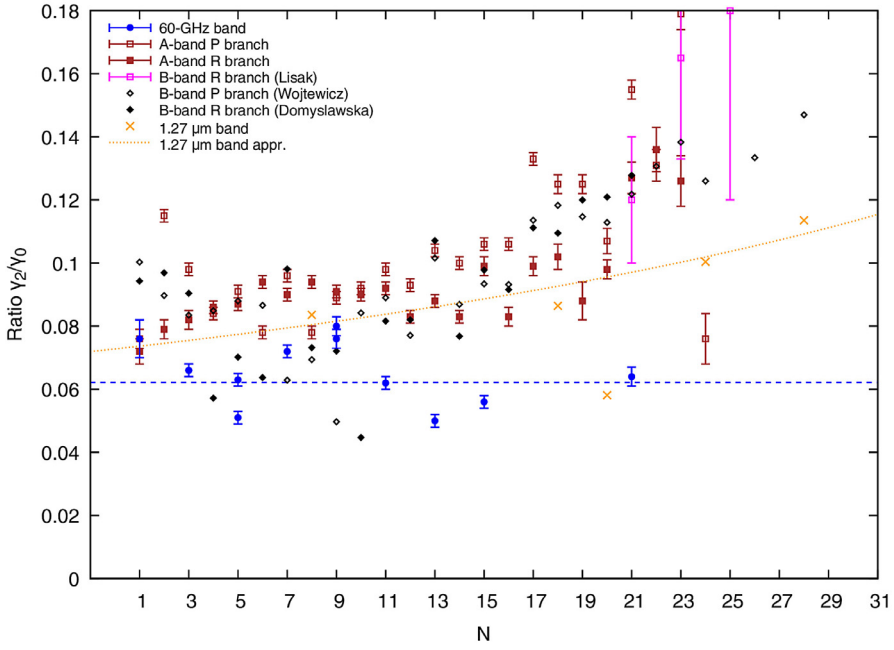

Fig. 6. Comparison of the γ_2/γ_0 ratio from the current study with data for the A-band [33], B-band [26–28] and 1.27 μm band [35]. The approximating function from [35] is shown by the orange dotted curve. Dashed line shows averaged ratio value 0.062(6) for the 60-GHz band.

cients to be revised. However, refining the model parameters is far beyond the scope of this study. Instead, we use a simplified approach to evaluate the impact of the SD effect on the 60-GHz band shape model, and the possibility of its experimental observation. The approach is based on a number of assumptions which are discussed below.

To achieve our goal the quadratic speed-dependent Van Vleck–Weisskopf line profile with corrections due to line mixing (qSDVVWLM [15]) was used:

$$\alpha(\nu) = \frac{S}{\pi}\left(\frac{\nu}{\nu_0}\right)^2 \int_0^\infty f_{MB}(v)\left(\frac{\Gamma(v) + Y(v)\cdot(\nu-\nu_0)}{(\nu-\nu_0)^2+\Gamma(v)^2} + \right.$$
$$\left. + \frac{\Gamma(v) - Y(v)\cdot(\nu+\nu_0)}{(\nu+\nu_0)^2+\Gamma(v)^2}\right) dv \qquad (4)$$

where S is the line intensity, $f_{MB}(v)$ is the Maxwell-Boltzmann speed distribution, $Y(v) = p\cdot y(v)$ is the first-order mixing parameter, and $\Gamma(v)$ is the collisional half-width with quadratic speed-dependence (2).

Eq. (4) neglects pressure shifting of the line center. This assumption is based on experimental data analysis [9,12,15] demonstrating that the effect does not manifest itself for the fine-structure lines. The shift parameter was estimated to be less than ±15 kHz/Torr for the 60-GHz band lines and less than ±4.5 kHz/Torr for the 1– line. This very low value allows us to neglect line shifting, including its speed dependence.

Fine-structure lines are quite similarly broadened by pressure of oxygen and nitrogen [9]. The ratios $\gamma/\gamma_0 = 0.992$ and $\gamma_2/\gamma_0 = 0.062$ discussed in Section 3 were adopted for all air-broadened lines of the band.

Recalling that (i) the y coefficient can be calculated as a weighted linear combination of off-diagonal elements of the collisional relaxation matrix and (ii) matrix elements follow the sum rule (see [5] for the details), we conclude that Y should also have quadratic speed dependence:

$$Y(v) = Y_0 + Y_2\left[\left(\frac{v}{\tilde{v}}\right)^2 - \frac{3}{2}\right] \qquad (5)$$

Moreover, we assume that $y/y_0 = \gamma/\gamma_0 = 0.992$ and $y_2/y_0 = \gamma_2/\gamma_0 = 0.062$ for all the lines. This is still an arbitrary assumption, because the broadening measurements have been made in pure O_2, and we don't know the temperature dependence of the y_2 parameters. But at least the assumption is consistent with Eq. (2) and with what we know about the relationship between line broadening and mixing. The uncertainty in y parameters thus obtained should produce a negligible effect on the band-shape modelling, considering that line mixing is normally a significantly smaller line-shape effect than line broadening.

The qSDVVWLM profile with coefficients Γ_0, Γ_2, Y_0 and Y_2 obtained as described above was introduced into the MPM to demonstrate the contribution of the SD effect to the shape of the 60-GHz band. (Note that the VVWLM profile is obtained from Eq. (4) assuming Γ_2 and Y_2 to be zero.) In addition, Eq. (4) was updated with second-order mixing corrections [5] (assumed to be speed independent) and included into the MPM code together with the mixing parameters from Makarov et al. [17]. Line intensities are interpreted as *a priori* known from the database [39] (as in the original MPM) and left unchanged. Eq. (4) is evaluated by numerical integration. This model is hereinafter referred to as SDMPM.

Before starting the analysis let us recall that the "impact" of any effect is usually demonstrated as a difference between model profiles: one *including the effect* and another one *neglecting the effect*. But even this difference can be demonstrated in two ways, comparing the "true" profile with a fitted one, or with a model based on *a priori* information on line shape parameters. We used both approaches to demonstrate the impact of the SD effect on the 60-GHz band profile.

Integrating Eq. (2) over a Maxwell–Boltzmann distribution of speeds yields Γ_0 as the averaged collisional broadening. In classical profiles (Van Vleck - Wesskopf (VVW), Voigt, Lorentz, *etc.*) Γ does not have such clear and certain physical meaning. It can be considered as an *ad hoc* parameter irrelevant to the molecular speed distribution. The qSDVVW(Γ_0, Γ_2) profile can be formally reduced to VVW(Γ_0) by setting Γ_2=0 and thus "switching off" the effect. However, the absorption calculated as qSDVVW(Γ_0, Γ_2=0) is different from that calculated as VVW(Γ) because of the difference between Γ and Γ_0 which can be up to 10% as found in other bands [27,34]. Moreover, collisional parameters (Γ, Γ_0, Γ_2) are usually determined from a fit of the corresponding line-shape function to the observed spectra. In most cases the line intensity S is assumed as a variable parameter and the fit result (for both width and intensity) depends on the line-shape model applied. Correlation of the line intensity and line width in the fitting introduces additional systematic differences between line profiles calculated by different line shape models when the line intensity is taken from an independent source.

4.1. Analysis of a single line

To demonstrate the aforesaid we start the analysis with a numerical simulation of a hypothetical single line at 1000 Torr. The line is modelled using the qSDVVWLM profile with Γ_0=2.274 GHz and Γ_2 = 0.172 GHz, corresponding to the experimental values for the $N = 1-$ line from Table 1 (at this pressure the lines near 60 GHz are not resolved; only the merged band profile is observed). For the other line shape parameters we set S=1, ν_0=100 GHz and $Y = 0$. So we assume at this step that the line is isolated and consider only the impact of SD-broadening. Fitting the VVW function to the simulated profile yielded ν_0=100 GHz, S=0.9981, Γ=2.253 GHz and a typical W-shape residual which is shown in Fig. 7, panel A. However, if we use the VVW function with the retrieved width Γ=2.253 GHz and initial intensity S=1, then the difference with the original profile becomes twice as large (red dashed curve). The solid red curve shows the difference between qSDVVW with non-zero and zero Γ_2 parameter. In both cases the difference increases significantly due to the fact that we consider both S and Γ as known parameters which are measured or calculated independently, as usually assumed in propagation models [1]. The dissimilarity of the solid and dashed red curves from the expected black W-shape residual is related to systematic errors in parameters retrieved using the inadequate line shape function. Both these red curves can be considered as the impact of the SD-broadening effect on the absorption profile. Later we will apply the same approach to evaluate the impact of the effect on the 60-GHz band shape.

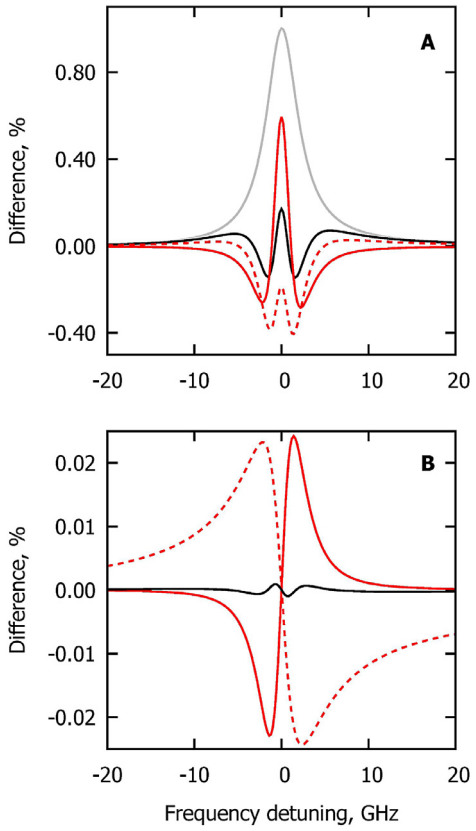

Fig. 7. Panel A: Manifestation of the SD-broadening effect for a single isolated line: the solid red curve is the impact of Γ_2=0 in the SD-model (eq. (4)) and the dashed red curve is the impact of replacing the classical Van Vleck-Weisskopf profile by the SD model. For comparison, the black curve is the residual from a Van Vleck-Weisskopf profile fitted to the SD-profile. The solid gray curve is the line profile with amplitude reduced by a factor of 100. Panel B: the same as A but for the partial contribution of the SD effect to collisional coupling. The solid red curve is the impact of Y_2=0 in the SD-model, the dashed red curve is the impact of first-order mixing reduced by a factor of 100, the black curve is the residual of the SDVVWLM profile from [15] fitted to the modeled profile including speed dependence of the mixing parameters. All curves are presented as the difference between models with and without the corresponding effect (see text for details).

Next we consider the impact of the SD-mixing in the first-order approximation. The values $Y_0 = -0.047461$ and $Y_2 = -0.003593$ at 1000 Torr were adopted for our hypothetical single line on the basis of the experimental value $y = 4.71 \cdot 10^{-5}$ 1/Torr and experimental ratios γ/γ_0 and γ_2/γ_0 for the 1− line, modelled using Eq. (4). The line profile employing the speed-dependence of $\Gamma(v)$ but neglecting the speed-dependence of $Y(v)$ from [15] was fitted to the modelled profile. The residual of this fit is shown in Fig. 7, panel B. Parameters retrieved from the fit are S=1.000016, ν_0=100.00079 GHz, Γ_0=2.2711 GHz, Γ_2=0.172 GHz and Y=-0.047443. Note the systematic difference from the initial Y value and shift of the line center. For comparison, the solid red curve shows the impact of setting $Y_2 = 0$ in the modelled profile and

the dashed red curve shows the contribution of the first-order line-mixing effect in the profile reduced by a factor of 100. The difference between the solid and the dashed red curves is more pronounced than between similar curves in panel A, due to the similar shape of the first-order mixing contribution to the impact of $Y_2 = 0$. This similarity allows the Y value to be adjusted in the velocity-independent model to account for most of the impact of the speed-dependence of $Y(v)$. Thus, even significant speed-dependence of the line mixing can be hidden, to a large extent, in experimental spectra. Interestingly, in this case setting Γ_2=0 results in a residual similar in its shape and amplitude to the solid red curve in panel A, which is independent of the Y_2 value. Calculations show that all curves in panel B scale linearly with Y. Typical values for the mixing parameters of the lines near 60 GHz are about an order of magnitude greater than the value used for the simulation. So the impact of SD-mixing on the band profile is expected to be comparable to the impact of the SD-broadening and cannot be neglected.

4.2. Analysis of the 60-GHz band

The difference between the 60-GHz band profile modelled with SDMPM and regular MPM at 750 Torr and 300 K in dry air is shown in Fig. 8. The magnitude of this difference is smaller than the first- and second-order mixing-effect contributions (note that the first-order mixing impact is shown reduced by a factor of 100 and the second-order by a factor of 10) and is of the order of the characteristic instrumental noise of our resonator spectrometer used for the band investigation (see [40] and references therein) with typical standard deviation σ=0.01 dB/km. Consequently, a direct detection of the SD effect in the band-profile recordings at atmospheric pressure seems impossible by means of contemporary measurement techniques. Note that the shape of the SD effect's contribution is similar to that of the first-order mixing contribution, although with the opposite sign and smaller magnitude.

Following the discussion in [19], the impact of the SD effect on the band can also be evaluated as a difference between SDMPM with known γ_0, γ_2, y_0, y_2 and the same model but with all γ_2 and

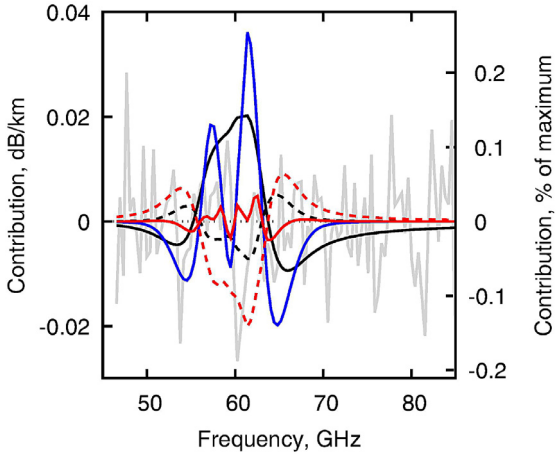

Fig. 8. Estimated contribution of the SD effect to the band shape at 750 Torr of dry air and 300 K. Dashed red curve is the impact of replacing the classical line shape model (with γ values from Tretyakov et al. [9] and Koshelev et al. [12]) by the SD model (with γ_0, γ_2, y_0 and y_2 calculated for all lines using data of this study). Dashed black and solid red curves are the result of setting y_2=0 and $\gamma_2 = y_2$=0 in the SD model, respectively. For comparison, a numerical simulation of a typical resonator spectrometer [40] noise trace (σ=0.01 dB/km, grey trace) and contributions of the first-order line mixing (solid black curve, amplitude reduced by factor of 100) and second-order line mixing (blue curve, amplitude reduced by factor of 10) are shown. All curves are presented as the difference between models with and without the corresponding effect.

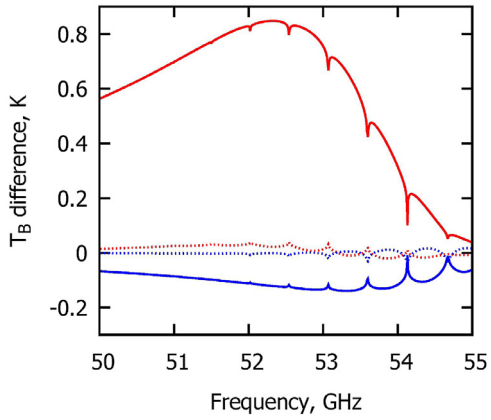

Fig. 9. Difference between brightness temperature using SDMPM and regular 2-nd order MPM [17]. Red curves correspond to the downwelling brightness temperature, blue curves for the upwelling one. Solid curves show the direct difference between brightness temperature calculated using regular MPM and SDMPM. Dotted curves show the impact of setting γ_2 and y_2 equal to zero in the SDMPM. U.S. Standard Atmosphere profile was used.

y_2 set to zero. This difference is presented in Fig. 8. In this case the magnitude of the difference is even smaller, and the "phase" (sign of maxima and minima at the band slopes) is opposite. The dashed black curve in Fig. 8, showing the influence of y_2 on the band profile, has a somewhat similar shape to the solid black curve for the contribution of the line mixing effect, but inverted. Line mixing transfers absorption toward the band center, and y_2 modifies that effect, although by less than 1%.

Thus when the lines forming the band overlap, as they do at 1-atm pressure, the influence of Γ_2 and Y_2 together is smaller than the difference between the SDMPM and MPM models (Fig. 8) which is mostly due to the difference between SD parameters Γ_0, Y_0 and VVWLM parameters Γ, Y. This weak influence on the band shape can be mimicked by the line mixing, which manifests itself by similar residuals (Fig. 8). Recall that line-mixing parameters are determined simultaneously for all fine-structure lines from the band profile recording at near to atmospheric pressures [6]. Thus direct experimental observation of the SD effect in the cumulative band profile seems impossible at the present state-of-the-art.

Small changes in the radiative transfer code can noticeably affect the calculated brightness temperature of the atmosphere, however, as shown in Fig. 9. The line-by-line microwave radiative transfer code [18] was used for the calculation together with the U.S. Standard Atmosphere profile for pressure, temperature and humidity. Code related to the oxygen absorption was modified as described above to consider the potential SD effect. The frequency range between 50 and 55 GHz is shown because of its relevance for remote sensing. In particular, significant biases between observations and radiative transfer simulations are known (see, *e.g.* [41] and references therein).

As discussed for Fig. 8, most of the observed difference is due to the difference between the γ_0, y_0 and γ, y parameters while the band intensity value does not change. Only small peaks located at the positions of the fine-structure lines demonstrate that the line shape model is different. It is very likely that most of this difference in the simulated brightness temperature will vanish after line-mixing parameters in the SDMPM are readjusted using laboratory recordings of the band profiles. Therefore, Fig. 9 should be interpreted as an upper limit to the possible changes.

5. Discussion and conclusions

Analysis of high-quality recordings of a number of the molecular oxygen fine-structure lines allowed determination of the SD

self-broadening parameters. The variation of the γ_2/γ_0 ratio with rotational quantum number N within the studied N range was weak. Extension of the known self-broadening parameters of the lines up to $N = 39$ allowed refinement of the self-broadening rotational dependence by means of a Padé approximation.

The impact of the SD effect on the 60-GHz band shape at atmospheric conditions was evaluated assuming a constant ratio $\gamma_2/\gamma_0 = y_2/y_0$ and $\gamma/\gamma_0 = y/y_0$ for all fine-structure lines and similar manifestation of the SD effect in air and pure O_2. The impact is about 100 and 10 times smaller than the first- and the second-order line-mixing effect, respectively. The shape of the effect manifested at atmospheric pressure is similar to first-order line mixing. It is thus very likely that most of the SD-related effect on the band profile near 1-atm pressure has already been taken into account by the mixing parameters which were determined from the experimental recordings at atmospheric pressure, thus hiding the SD-effect manifestation.

At atmospheric pressure, the impact of speed dependence on line mixing for the 60-GHz band is comparable to the impact on line broadening, but both are small.

The question of the band intensity is relevant. Further updates of the band model should come together with verified intensities of the fine-structure lines, to allow better determination of the mixing parameters after implementation of the speed-dependent line shape and corresponding broadening parameters.

Declaration of Competing Interest

The authors declare that they have no known competing financial interests or personal relationships that could have appeared to influence the work reported in this paper.

CRediT authorship contribution statement

M.A. Koshelev: Methodology, Formal analysis, Writing - original draft, Writing - review & editing. **I.N. Vilkov:** Investigation, Data curation. **D.S. Makarov:** Visualization, Software. **M.Yu. Tretyakov:** Supervision, Conceptualization, Writing - review & editing. **P.W. Rosenkranz:** Conceptualization, Writing - review & editing.

Acknowledgements

The study was supported by RFBR (grant 19-05-00969). Investigation of the weak lines was performed under the support of the Russian Science Foundation (project 17-19-01602).

References

[1] Cimini D, Rosenkranz PW, Tretyakov MYu, Koshelev MA, Romano F. Uncertainty of atmospheric microwave absorption model: impact on ground-based radiometer simulations and retrievals. Atmos Chem Phys 2018;18(20):15231–59.
[2] Rosenkranz PW. Shape of the 5 mm oxygen band in the atmosphere. IEEE Trans Antennas Propag 1975;23(4):498–506.
[3] Gordon RG. On the pressure broadening of molecular multiplet spectra. J Chem Phys 1967;46(2):448–55.
[4] Liebe HJ, Gimmestad GG, Hopponen JD. Atmospheric oxygen microwave spectrum - experiment versus theory. IEEE Trans Antennas Propag 1977;25(3):327–35.
[5] Smith EW. Absorption and dispersion in the O_2 microwave spectrum at atmospheric pressures. J Chem Phys 1981;74(12):6658–73.
[6] Rosenkranz PW. Interference coefficients for overlapping oxygen lines in air. J Quant Spectrosc Radiat Transf 1988;39:281–97.
[7] Liebe HJ, Rosenkranz PW, Hufford GA. Atmospheric 60-GHz oxygen spectrum: new laboratory measurement and line parameters. J Quant Spectrosc Radiat Transf 1992;48(5,6):629–43.
[8] Makarov DS, Tretyakov MYu, Boulet C. Line mixing in the 60-GHz atmospheric oxygen band: Comparison of the MPM and ECS model. J Quant Spectrosc Radiat Transf 2013;124:1–10.
[9] Tretyakov MYu, Koshelev MA, Dorovskikh VV, Makarov DS, Rosenkranz PW. 60-GHz oxygen band: precise broadening and central frequencies of fine structure lines, absolute absorption profile at atmospheric pressure, revision of mixing coefficients. J Molec Spectrosc 2005;231:1–14.
[10] Makarov DS, Koval IA, Koshelev MA, Parshin VV, Tretyakov MYu. Collisional parameters of the 118-GHz oxygen line: temperature dependence. J Molec Spectrosc 2008;252:242–3.
[11] Koshelev MA, Vilkov IN, Tretyakov MYu. Pressure broadening of oxygen fine structure lines by water. J Quant Spectrosc Radiat Transf 2015;154:24–7. doi:10.1016/j.jqsrt.2014.11.019.
[12] Koshelev MA, Vilkov IN, Tretyakov MYu. Collisional broadening of oxygen fine structure lines: the impact of temperature. J Quant Spectrosc Radiat Transf 2016;169:91–5.
[13] Tretyakov MYu, Golubiatnikov GYu, Parshin VV, Koshelev MA, Myasnikova SE, Krupnov AF, et al. Experimental study of the line mixing coefficient for 118.75 GHz oxygen line. J Molec Spectrosc 2004;223:31–8.
[14] Tretyakov MYu, Koshelev MA, Koval I, Parshin VV, Kukin LM, Fedoseev LI, et al. Temperature dependence of pressure broadening of the $N = 1-$ fine structure oxygen line at 118.75 GHz. J Molec Spectrosc 2007;241(1):109–11.
[15] Koshelev MA, Delahaye T, Serov EA, Vilkov IN, Boulet C, Tretyakov MYu. Accurate modeling of the diagnostic 118-GHz oxygen line for remote sensing of the atmosphere. J Quant Spectrosc Radiat Transf 2017;196:78–86. doi:10.1016/j.jqsrt.2017.03.043.
[16] Makarov DS, Tretyakov MYu, Rosenkranz PW. 60-GHz oxygen band: precise experimental profiles and extended absorption modeling in a wide temperature range. J Quant Spectrosc Radiat Transf 2011;112(9):1420–8.
[17] Makarov DS, Tretyakov MYu, Rosenkranz PW. Revision of the 60-GHz atmospheric oxygen absorption band models for practical use. J Quant Spectrosc Radiat Transf 2020;243:106798. doi:10.1016/j.jqsrt.2019.106798.
[18] Rosenkranz P.W.. Line-by-line microwave radiative transfer (non-scattering). 2017. doi: 10.21982/M81013.
[19] Rosenkranz PW, Cimini D. Speed dependence of 22- and 118-GHz line shapes for tropospheric remote sensing. IEEE Trans Geosci Remote Sens 2019;57(12):9702–8. doi:10.1109/TGRS.2019.2928570.
[20] Tretyakov MYu, Koshelev MA, Makarov DS, Tonkov MV. Precise measurements of collision parameters of spectral lines with a spectrometer with radioacoustic detection of absorption in the millimeter and submillimeter ranges. Instrum Exp Tech 2008;51(1):78–88.
[21] Koshelev MA, Golubiatnikov GYu, Vilkov IN, Tretyakov MYu. Line shape parameters of the 22-GHz water line for accurate modeling in atmospheric applications. J Quant Spectrosc Radiat Transf 2018;205:51–8. doi:10.1016/j.jqsrt.2017.09.032.
[22] Ngo N, Lisak D, Tran H, Hartmann J-M. An isolated line-shape model to go beyond the Voigt profile in spectroscopic databases and radiative transfer codes. J Quant Spectrosc Radiat Transf 2013;129:89–100. doi:10.1016/j.jqsrt.2013.05.034.
[23] Tennyson J, Bernath PF, Campargue A, Császár AG, Daumont L, Gamache RR, et al. Recommended isolated-line profile for representing high-resolution spectroscopic transitions (IUPAC technical report). Pure Appl Chem 2014;86:1931–43. doi:10.1515/pac-2014-0208.
[24] Rohart F, Mader H, Nicolaisen H-W. Speed dependence of rotational relaxation induced by foreign gas collisions: studies on CH_3F by millimeter wave coherent transients. J Chem Phys 1994;101(8):6475–86.
[25] Rohart F, Ellendt A, Kaghat F, Mäder H. Self and polar foreign gas line broadening and frequency shifting of CH_3F: effect of the speed dependence observed by millimeter-wave coherent transients. J Molec Spectrosc 1997;185(2):222–33.
[26] Lisak D, Masłowski P, Cygan A, Bielska K, Wójtewicz S, Piwiński M, et al. Line shapes and intensities of self-broadened $O_2 b^1\Sigma_g^+(v=1) \leftarrow x^3\Sigma_g^-(v=0)$ band transitions measured by cavity ring-down spectroscopy. Phys Rev A 2010;81:042504. doi:10.1103/PhysRevA.81.042504.
[27] Wójtewicz S, Cygan A, Masłowski P, Domysławska J, Lisak D, Trawiński R, et al. Spectral line shapes of self-broadened P-branch transitions of oxygen B-band. J Quant Spectrosc Radiat Transf 2014;144:36–48. doi:10.1016/j.jqsrt.2014.03.029.
[28] Domysławska J, Wójtewicz S, Masłowski P, Cygan A, Bielska K, Trawiński RS, et al. A new approach to spectral line shapes of the weak oxygen transitions for atmospheric applications. J Quant Spectrosc Radiat Transf 2016;169:111–21. doi:10.1016/j.jqsrt.2015.10.019.
[29] Brown L, Plymate C. Experimental line parameters of the oxygen A band at 760 nm. J Molec Spectrosc 2000;199(2):166–79. doi:10.1006/jmsp.1999.8012.
[30] Predoi-Cross A, Hambrook K, Keller R, Povey C, Schofield I, Hurtmans D, et al. Spectroscopic lineshape study of the self-perturbed oxygen A-band. J Molec Spectrosc 2008;248(2):85–110. doi:10.1016/j.jms.2007.11.007.
[31] Long D, Havey D, Yu S, Okumura M, Miller C, Hodges J. O_2 A-band line parameters to support atmospheric remote sensing. Part II: the rare isotopologues. J Quant Spectrosc Radiat Transf 2011;112(16):2527–41. doi:10.1016/j.jqsrt.2011.07.002.
[32] Gordon IE, Rothman LS, Hill C, Kochanov RV, Tan Y, Bernath PF, et al. The HITRAN2016 molecular spectroscopic database. J Quant Spectrosc Radiat Transf 2017;203:3–69.
[33] Drouin BJ, Benner DC, Brown LR, Cich MJ, Crawford TJ, Devi VM, et al. Multispectrum analysis of the oxygen A-band. J Quant Spectrosc Radiat Transf 2017;186:118–38. doi:10.1016/j.jqsrt.2016.03.037.
[34] Domysławska J, Wójtewicz S, Masłowski P, Cygan A, Bielska K, Trawiński RS, et al. Spectral line shapes and frequencies of the molecular oxygen B-band R-branch transitions. J Quant Spectrosc Radiat Transf 2015;155:22–31. doi:10.1016/j.jqsrt.2014.12.015.
[35] Konefał M, Kassi S, Mondelain D, Campargue A. High sensitivity spectroscopy of the O_2 band at 1.27 μm: (i) pure O_2 line parameters above 7920 cm^{-1}. J Quant Spectrosc Radiat Transf 2020;241:106653. doi:10.1016/j.jqsrt.2019.106653.

[36] Koshelev MA, Tretyakov MYu, Rohart F, Bouanich J-P. Speed dependence of collisional relaxation in ground vibrational state of OCS: rotational behaviour. J Chem Phys 2012;136(12):124316–(111).
[37] Koshelev MA, Vilkov IN, Makarov DS, Tretyakov MYu, Vispoel B, Gamache RR, et al. Water vapor line profile at 183-GHz: temperature dependence of broadening, shifting, and speed-dependent shape parameters. J Quant Spectrosc Radiat Transf 2021;262:107472.
[38] Rosenkranz PW. Line-by-line microwave radiative transfer (non-scattering) at an international network of ground-based microwave radiometers. online access to the code http://cetemps.aquila.infn.it/mwrnet/lblmrt_ns.html.
[39] Rothman LS, Jacquemart D, Barbe A, Benner DC, Birk M, Brown LR, et al. The HITRAN2004 molecular spectroscopic database. J Quant Spectrosc Radiat Transf 2005;96(2):139–204.
[40] Koshelev MA, Leonov II, Serov EA, Chernova AI, Balashov AA, Bubnov GM, et al. New frontiers in modern resonator spectroscopy. IEEE Trans Terahertz Sci Technol 2018;8(6):773–83. doi:10.1109/TTHZ.2018.2875450.
[41] De Angelis F, Cimini D, Löhnert U, Caumont O, Haefele A, Pospichal B, et al. Long-term observations minus background monitoring of ground-based brightness temperatures from a microwave radiometer network. Atmos Meas Tech 2017;10:3947–61. doi:10.5194/amt-10-3947-2017.